Eur Radiol (2004) 14:309–317
DOI 10.1007/s00330-003-2025-2

Heinz-Peter Schlemmer
Jonas Merkle
Rainer Grobholz
Tim Jaeger
Maurice Stephan Michel
Axel Werner
Jan Rabe
Gerhard van Kaick

Can pre-operative contrast-enhanced dynamic MR imaging for prostate cancer predict microvessel density in prostatectomy specimens?

Received: 14 November 2002
Revised: 16 May 2003
Accepted: 20 June 2003
Published online: 3 October 2003

H.-P. Schlemmer (✉) · J. Merkle
G. van Kaick
Department of Oncological Diagnostics and Therapy,
German Cancer Research Center,
University Hospital Mannheim,
Ruprecht Karls University, Heidelberg, Germany
e-mail: heinz-peter.schlemmer@med.uni-tuebingen.de
Tel.: +49-7071-2982087
Fax: +49-7071-295392

R. Grobholz
Department of Pathology,
University Hospital Mannheim,
Ruprecht Karls University,
Heidelberg, Germany

T. Jaeger · M. S. Michel
Department of Urology,
University Hospital Mannheim,
Ruprecht Karls University,
Heidelberg, Germany

A. Werner · J. Rabe
Department of Diagnostic Radiology,
University Hospital Mannheim,
Ruprecht Karls University,
Heidelberg, Germany

H.-P. Schlemmer
Department of Diagnostic Radiology,
University Hospital Tuebingen,
Hoppe-Seyler-Strasse 3, 72076 Tuebingen,
Germany

Abstract The aim of this study was to correlate quantitative dynamic contrast-enhanced MRI (DCE MRI) parameters with microvessel density (MVD) in prostate carcinoma. Twenty-eight patients with biopsy-proven prostate carcinoma were examined by endorectal MRI including multiplanar T2- and T1-weighted spin-echo and dynamic T1-weighted turbo-FLASH MRI during and after intravenous Gd-DTPA administration. Microvessels were stained on surgical specimens using a CD31 monoclonal antibody. The MVD was quantified in hot spots by counting (MVC) and determining the area fraction by morphometry (MVAF). The DCE MRI data were analyzed using an open pharmacokinetic two-compartment model. In corresponding anatomic locations the time shift (Δt) between the beginning of signal enhancement of cancer and adjacent normal prostatic tissue, the degree of contrast enhancement and the contrast exchange rate constant (k_{21}) were calculated. The MVC and MVAF were elevated in carcinoma ($p<0.001$ and $p=0.002$, respectively) and correlated to k_{21} ($r=0.62$, $p<0.001$ and $r=0.80$, $p<0.001$, respectively). k_{21}-values of carcinoma were significantly higher compared with normal peripheral but not central zone tissue. Δt was longer in high compared with low-grade tumors ($p=0.025$). The DCE MRI can provide important information about individual MVD in prostate cancer, which may be helpful for guiding biopsy and assessing individual prognosis.

Keywords Prostate carcinoma · Dynamic contrast-enhanced MR imaging · Angiogenesis · Microvessel density

Introduction

Prostate cancer has become a leading cause of morbidity and mortality in men in Western countries. The risk of developing clinical disease is presently assessed at approximately 13% [1]. In the next decades the increasing natural life expectation will result in a further increase of both the incidence of prostatic cancer as well as the related death rate [2].

The main diagnostic problems for clinicians concerned with prostate cancer include early detection, localization, and staging, as well as prediction of individual aggressiveness. For curative treatment the identification of early tumor stage in asymptomatic individuals is

crucial. Early detection was significantly improved using prostate-specific antigen (PSA) serum testing, and the rapid increase of prostate cancer incidence during the past two decades can partially be explained by this serum test [3]. It is furthermore encouraging that the frequency of cancers in the preinvasive phase with tumor spread confined to the prostate has continuously increased using PSA screening. In any case, however, systematic needle biopsy is performed to finally confirm the presence of cancer and to assess the tumor grade.

The preferred treatment of early stage cancer confined to the prostate is radical prostatectomy or conformal radiotherapy. To select patients for radical prostatecomy accurate preoperative staging is important, particularly for identification of extracapsular extension, seminal vesicle invasion, and distant tumor spread to avert unnecessary surgery. The most commonly used clinical parameters for assessing the probability of organ confined disease include digital rectal examination, PSA serum level, and the Gleason grading after systematic sextant biopsy of the prostate. Transrectal ultrasound (TRUS) is essentially important for guiding biopies of the prostate in patients suspected of having prostate cancer. After histological confirmation MR imaging with an endorectal surface coil (endoMRI) offers the most promise for local staging, particularly for ruling out extraprostatic tumor extension and seminal vesicle infiltration. The reported staging accuracy of endoMRI for predicting extracapsular or seminal vesicle involvement varies from approximately 50 to 80% with considerable interreader variability [4, 5]. Jager et al. [6] have shown that endoMRI can be cost-effective in the presurgical evaluation of men with moderate or high prior probability of extracapsular disease, particularly to avert unnecessary radical prostatectomy. Disadvantages of endoMRI are due to its low specificity, but staging accuracy can be improved by adding 3D proton MR spectroscopic imaging to the routine MRI protocol [7].

Even though desirable, however, there is presently no reliable capability to discriminate between latent and potentially aggressive tumors. Much research has gone into the prognostic factors that can predict outcome in individual patients with prostate cancer. According to the Consensus Statements of the College of American Pathologists in 1999 prognostic factors in prostate cancer are divided into three categories [8]. Category 1 includes factors that proved to be of prognostic importance (e.g., serum PSA level, TNM staging, Gleason grading). Category-2 factors are extensively studied, but the clinical value has to be validated in statistically robust studies (e.g., tumor volume, DNA ploidy). Category-3 factors have been shown to be promising but are not yet studied well enough; of those, microvessel density and neuroendocrine differentiation are particularly promising.

Several studies have showed that tumor neovascularization is correlated with an increased risk of distant metastases and tumor recurrence after surgery as well as poorer overall survival [9, 10, 11, 12]. The aim of this study was to evaluate the potential of fast dynamic, contrast-enhanced T1-weighted MR imaging to predict microvessel density in prostate cancer for improved tumor localization and characterization. For this purpose tumor microvessel density was correlated with parameters characterizing the kinetics of contrast enhancement.

Patients and methods

Twenty-eight patients (mean age 63.0 years**,** age range 56–70 years) with clinically localized and biopsy-confirmed prostate cancer designated for radical retropubic prostatectomy were included in this study. Informed consent was obtained in each patient. The TRUS (without color Doppler or contrast enhancement) was carried out in all patients and showed suspicious findings in 25 cases. Serum levels of PSA and vascular endothelial growth factor (VEGF) were determined preoperatively. Radical retropubic prostatectectomy was conducted within 1 week after MRI.

MR imaging

Magnetic resonance imaging examinations were performed in consecutive patients between June 1999 and April 2000 using a 1.0-T MR scanner (Magnetom Harmony, Siemens, Erlangen, Germany) and a combined endorectal-body phased-array coil (Medrad, Maastricht, The Netherlands). The DCE MRI was performed and evaluated without knowledge of the TRUS findings. Time interval between biopsy and DCE MRI was 49.7±31.4 days (range 13–135 days). It was in 25 of 28 patients longer than 3 weeks, which was shown to less likely affect staging accuracy [13]. Just before MR imaging, 40 mg of hyoscine butylbromide (Buscopan, Boehringer, Ingelheim, Germany) was administered intravenously in all patients to suppress rectal peristalis.

Prostate and seminal vesicles were imaged using axial and coronal T2-(TR/TE=4400 ms/120 ms) and axial T1-weighted (TR/TE=700 ms/12 ms) turbo-spin-echo sequences with 3-mm section thickness, 0.3-mm intersection gap, field of view (FOV) 200 mm, and matrix size 225×256. Dynamic, contrast-enhanced MR imaging was performed using an inversion recovery turbo fast low-angle shot (FLASH) sequence (TR/TE=1300 ms/4.2 ms, effective inversion time (TI) 654 ms, flip angle 13°, FOV 360 mm, matrix size 128×128). Ten slices with 4-mm slice thickness and 0.8-mm intersection gap were subsequently recorded leading to an acquisition time of 13 s for each repetition. In total, 22 repetitions were acquired. With beginning of the third repetition 0.1 mmol/kg of gadopentetate dimeglumine (Magnevist, Schering, Berlin, Germany) was injected through a cubital vein by a short constant rate infusion within 30 s using a variable-speed infusion pump (Spectris MR Injector, Medrad, Maastricht, The Netherlands).

Histopathological analysis

Prostatectomy specimens were fixed in 10% neutral buffered formalin for 24 h. The organ was completely sliced and paraffin embedded according standard protocols so that anatomical regions could be easily reproduced [14]. Briefly, four- to five-step sections (8 mm) were made in a plane perpendicular to the long axis of the urethra, which corresponded to the sections used for axial MR imaging. Each slice was cut in half according to the right and left side of each lobe. The ventral and dorsal segments were embedded

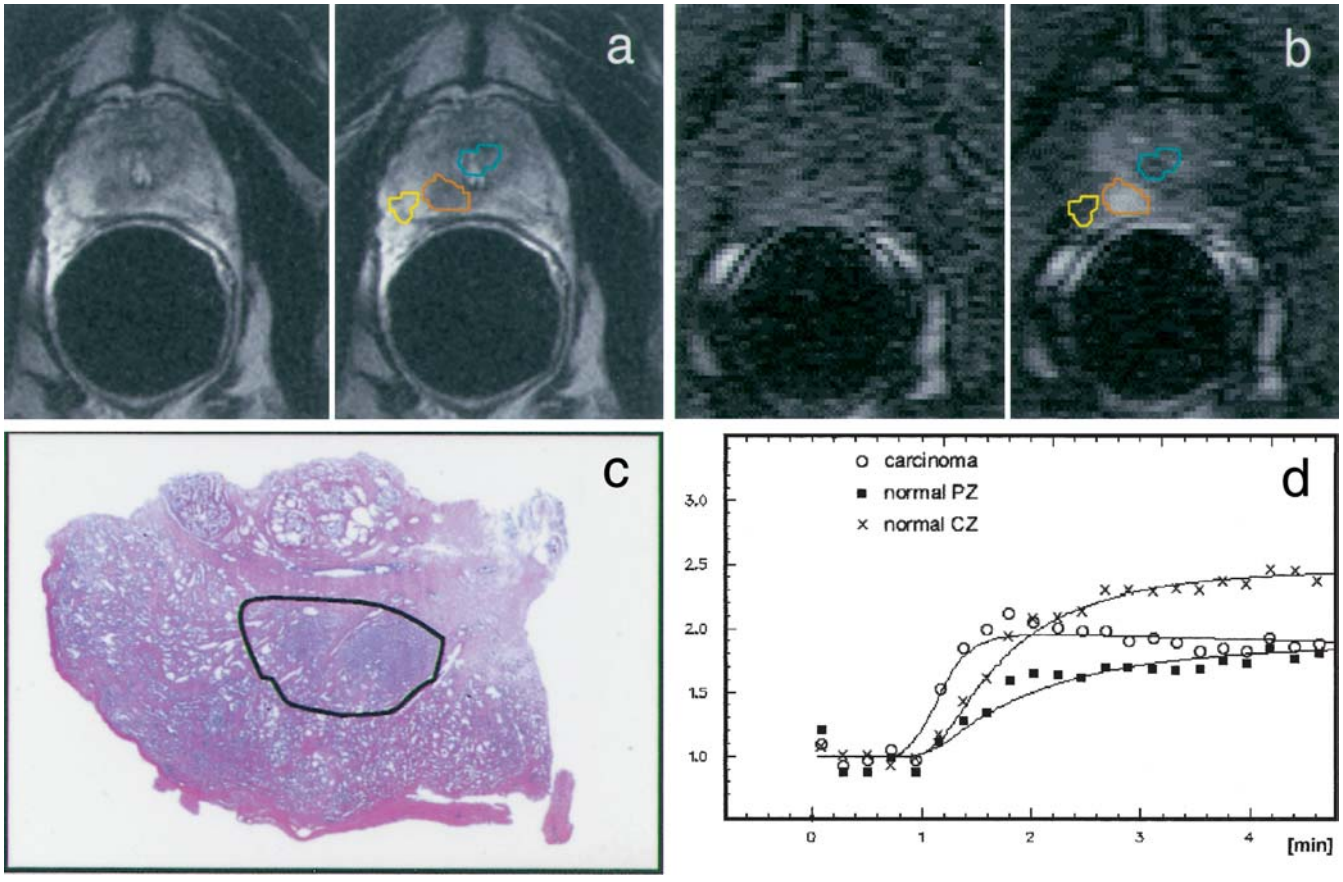

Fig. 1 **a** Axial T2-weighted MR image (turbo-spin-echo sequence, TR/TE=4400 ms/120 ms) showing organ-confined carcinoma in the right peripheral zone as circumscribed low signal intensity area. **b** Dynamic contrast-enhanced MR-image (turbo FLASH, TR/TI/TE=1300 ms/654 ms/4.2 ms) before and approximately 1 min after start of intravenous contrast medium application demonstrating fast signal enhancement of the tumor area compared with normal peripheral zone (PZ) and central zone (CZ). Operator-defined irregular regions of interest (ROIs) outlining areas of carcinoma (*red*) as well as adjacent normal PZ (*yellow*) and CZ (*green*) are displayed on corresponding images on the right. **c** Prostatectomy specimen of the dorsal segment of the right lobe showing tumor bulk within the right peripheral zone. **d** Signal–time curves of selected ROIs demonstrating signal enhancement characteristics of carcinoma compared with normal PZ and CZ

separately and numbered consecutively from the apical to the basal regions, so that the location of each lesion within the prostate could be accurately noted. Sections of tumor tissue were stained with hematoxylin and eosin for tumor classification according to the International Union against Cancer TNM classification, 5th edition, 1997. The grading was performed according to Gleason and Mellinger [15]. Regions representing the main tumor bulk were determined by light microscopy as outlined on the glass cover. Small areas of histological multifocal tumors were not included in the study. High-grade tumors correlated to Gleason scores 7–10, low-grade tumors to Gleason scores 2–6. One pathologist (R.G.) reviewed all cases for the present study.

Immunohistochemistry

For detection of antigenic sites a biotin–streptavidin amplified indirect immunoperoxidase method was used as described previously [16]. Briefly, 3-µm-thick serial sections were cut in a SM200R microtome (Leica, Nussloch, Germany) and deparaffinized using standard protocols. Antigen retrieval was performed in a microwave oven at 900 W 3×5 min in a citrate buffer (pH=6.0). For demonstration of CD31 a monoclonal antibody (Dako, Hamburg, Germany) was used at a 1:20 dilution and an overnight incubation at 4°C in a dark humid incubation chamber. The secondary antibody was applied for 30 min and the streptavidin–alkaline phosphatase conjugated complex (Dianova, Hamburg, Germany) was added for 30 min after washing in TBS. The use of the substrate naphthol with the chromogen Fast Red (Boehringer, Mannheim, Germany) resulted in a red amorphous precipitate at the binding site. Counterstaining was performed with Mayer's hematoxylin (Merck, Darmstadt, Germany). Sections for morphometrical evaluation were not counterstained. Slides were mounted in Kaiser's glycerin gelatine (Merck, Darmstadt, Germany). Incubation with preimmune serum, instead of the primary antibody, served as negative control.

Microvessel density

Microvessel density was assessed as described previously [17] by light microscopy in areas of invasive tumor containing the highest numbers of capillaries per area ("hot spots"). Areas of highest neovascularization were found by scanning the tumor at low magnification and identifying those areas of invasive carcinoma with the greatest number of microvessels per area. Individual microvessel

counts (MVC) were made on a ×200 field (×20 objective and ×10 ocular, 0.74 mm^2 per field) or by using a 10×10 square ocular grid (0.16 mm^2). Three individual fields were counted per hot spot.

Morphometry was carried out in a modified and adapted method as previously published [16]. Vascular density was determined with the aid of a Leitz Orthoplan microscope (Leica, Bensheim, FRG) coupled to a RGB camera (Leica, Bensheim, Germany) following visualization on a high-resolution display monitor (Leica, Bensheim, Germany) combined with the semi-automatic image analyzing system Quantimed Q500MC (Leica, Bensheim, Germany). To measure vascular area, a threshold level was set so that objects other than the selected color scale were illuminated, distinguishing between objects of positive immunoreactivity and the counterstained background. The area (μm^2) of all highlighted objects was measured by the computer in the designated field. Within the designated tumor region the area of microvessels in five fields of tumorous and the surrounding non-tumorous tissue of the tissue block was measured at a 40-fold magnification (×4 objective and ×10 ocular). The mean area of microvessels of these five fields was calculated, and subsequently, the area fraction (%) was determined as the mean vascular area per measure field (MVAF). For the evaluation of the vascular area a computer program was used, supplied with the Quantimed Q500MC (Leica, Bensheim, Germany).

Image analysis

Dynamic data were analyzed retrospectively on a separate workstation (VAX Alpha 3000/500, Digital Equipment Co., Maynard, Mass.). For each patient one histopathological section showing the main tumor bulk within the peripheral zone was selected, and the tumor region was identified on anatomically corresponding T2-weighted and DCE MR images. Contrast dynamic parameters were evaluated from signal–time curves obtained in operator defined, irregular regions of interests (ROIs) outlining areas of cancer and adjacent normal tissue. The selection of ROIs was performed in cooperation with one radiologist (H.P.S.) and one pathologist (R.G.) both having special expertise in prostate cancer imaging and pathology, respectively. Location, size, and shape of the ROIs corresponded to the main tumor bulk and the surrounding normal tissue shown on histopathological specimens (Fig. 1a–c). Dynamic data were analyzed by a least-squares fitting routine and a pharmacokinetic open two-compartment model providing the parameters degree of signal enhancement (amplitude, A) and exchange rate constant [k_{21} (min^{-1})] [18, 19]. Additionally, the time shift (Δt) between the beginning of the signal enhancement of cancer and adjacent normal tissue was calculated. A software package developed by Hoffmann et al. was used for data postprocessing [20].

Statistical analysis

Statistical analysis was performed using SAS software (SAS for Windows, version 6.12). Proof of significance was performed using Student's *t* test. The *p* values <0.05 were considered to be significant. The association between the pharmacokinetic parameters (A and k_{21}) and microvessel density was assessed by calculating linear correlation coefficient.

Results

Dynamic contrast-enhanced MRI examinations of all 28 patients could be evaluated. Pathological confirmed cancer areas in the peripheral zone of the prostate were characterized by low signal on T2-weighted MR images in 22 of 28 cases (79%) or pronounced contrast enhancement in 19 of 28 cases (68%). In 25 of 28 of the cases (89%) tumors could be depicted either on T2-weighted and/or DCE MR images.

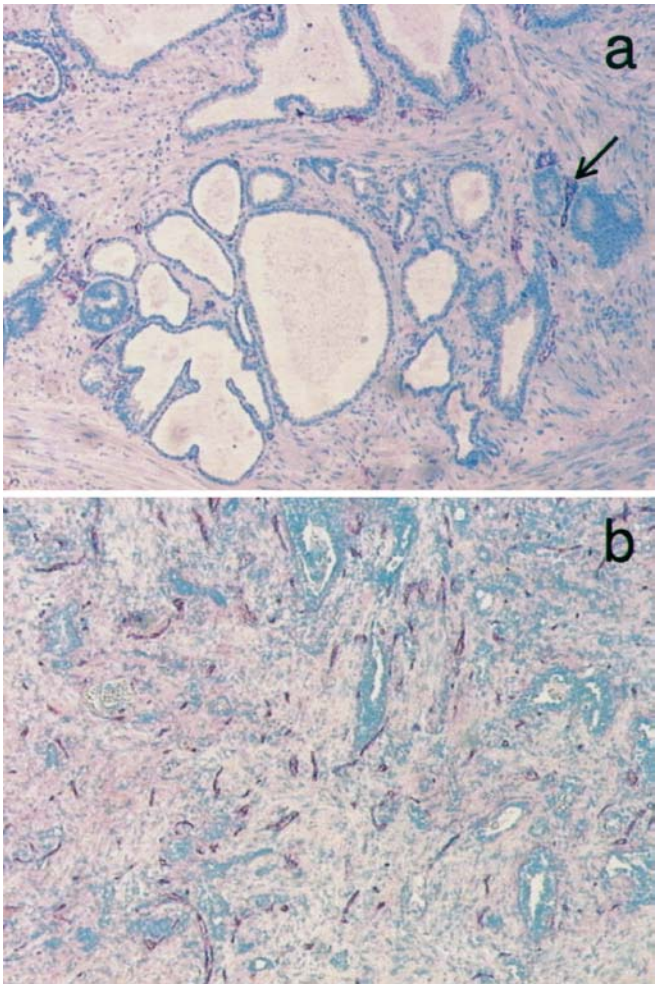

Fig. 2a, b Prostatectomy specimen demonstrating microvessels (*red*, *arrow*) in **a** benign prostatic tissue and **b** tumor tissue by staining of CD 31. Significantly more microvessels are found in tumor tissue than in the surrounding non-neoplastic tissue. Original magnification ×12.5

Representative ROIs outlining areas of carcinoma and adjacent normal tissue together with the obtained signal–time curves are illustrated in Fig. 1. The ROIs within regions of normal peripheral zone (PZ) and central zone (CZ) could be defined in 26 cases. In 2 cases normal prostate tissue was found only in the central zone, because the peripheral zone was completely infiltrated by tumor tissue.

Pathological local tumor stage was pT_2 in 12 patients, pT_3 in 15 patients, and pT_4 in 1 patient. Thirteen patients had low-grade tumors and 15 patients had high-grade tumors. Microvessels staining positive for CD 31 were present in variable amounts in all sections studied with an emphasis on the tumor compartment (Fig. 2). The

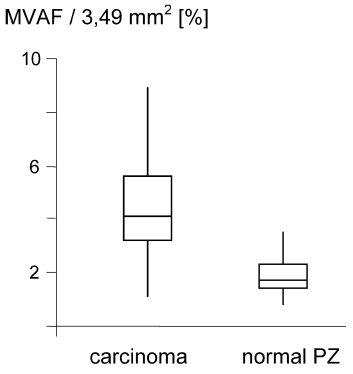

Fig. 3 Box-Whisker plots of microvessel density determined as the mean vascular area per measure field (MVAF) observed in areas of cancer and normal peripheral zone. The *center horizontal line* indicates the median, the bottom and top edges of the box the 25th and 75th percentiles. The *vertical line* measures the range of data. Significantly higher values of MVAF are observed in cancer areas (p=0.002)

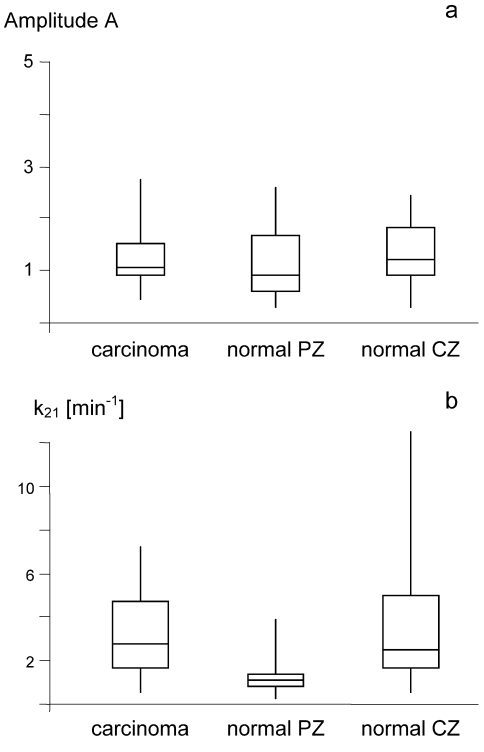

Fig. 4a, b Box-Whisker plots of **a** amplitude (A) and **b** exchange rate constant (k_{21}) obtained from ROIs outlining histopathologically proven areas of carcinoma, and adjacent normal PZ and CZ. Values of k_{21} are significantly elevated in carcinoma compared with normal PZ (p=0.008), whereas values from carcinoma and CZ do not differ. No significant differences of A-values are found

mean area fraction of microvessels in the surrounding non-neoplastic prostate tissue was significantly lower than in tumor tissue (1.71±0.62 vs 4.33±1.90%, p=0.002; Fig. 3). The mean vessel count in tumor tissue was 93.4±30.1 for all tumors. High- and low-grade tumors

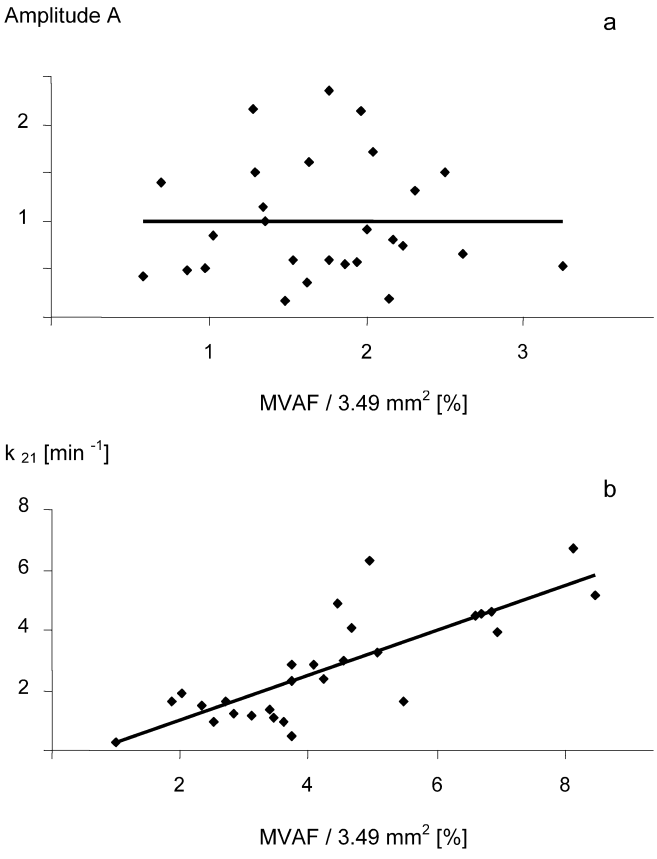

Fig. 5 **a** *Amplitude A* and **b** exchange rate constant (k_{21}) obtained from carcinoma ROIs as a function of microvessel density determined as the mean vascular area fraction. Values of k_{21} and microvessel density are correlated (r=0.80, p<0.001)

Table 1 Mean and standard deviation of the degree of signal enhancement (amplitude, A) and the exchange rate constant [k_{21}, (min^{-1})] obtained in carcinoma, normal peripheral zone (*PZ*), and normal central zone (*CZ*) of the prostate. Data were calculated from signal–time curves using a least-squares fitting routine and a pharmacokinetic open two-compartment model

	Carcinoma	PZ	CZ
A	1.09±0.50	0.99±0.60	1.18±0.55
k_{21}	2.75±1.77	0.98±0.80	3.29±2.58

exhibited a mean area fraction (MVAF) of 4.36±1.84 and 4.30±1.84% (p=0.93) as well as a microvessel count (MVC) of 98±19.1 and 88±38.6 (p=0.43), respectively.

Calculated pharmacokinetic parameters A and k_{21} are given in Table 1 and plotted in Fig. 4. k_{21}-values of carcinoma were significantly elevated compared with values of normal PZ (p=0.008). In contrast, k_{21}-values of carcinoma and normal CZ did not differ. Additionally, no differences were found between A-values of carcinoma, normal PZ, and normal CZ.

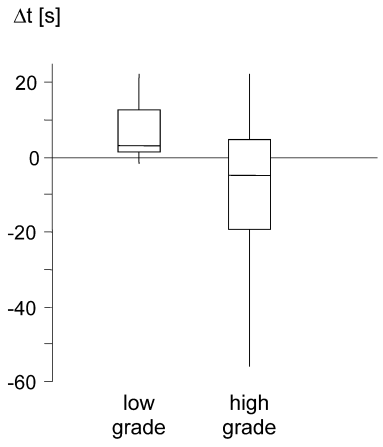

Fig. 6 Box-Whisker plots of relative time shifts (Δt) between the beginning of signal enhancement in areas of normal PZ and low-grade (Gleason score ≤6; n=13) as well as high-grade tumors (Gleason score ≥7; n=15). Positive (negative) values indicate later (earlier) enhancement of the tumor compared with the adjacent PZ. In high-grade tumors signal enhancement starts significantly earlier than in low-grade tumors (–9.0±22.9 vs 6.4±7.2 s; p=0.025)

A correlation was found between k_{21} and MVD. The correlation coefficient was higher for MVD values evaluated by semi-automatic image analyzing (MVAF**;** r=0.80; p<0.001) than for MVD values evaluated by counting (MVC**;** r=0.62; p<0.001). No correlation was found between MVC/MVAF and A (r=-0.26/–0.22; Fig. 5). Additionally, neither values of MVC/MVAF nor pharmacokinetic parameters A/k_{21} were correlated with T stage (r=-0.16/–0.33 and r=0.08/–0.20), Gleason grade (r=0.28/0.11 and r=–0.01/0.05) or serum levels of PSA (r=–0.13 /0.07 and r=0.13/0.11) and VEGF (r=0.10/–0.08 and r=0.10/–0.08). Comparing low-grade (Gleason score ≤6; n=13) and high-grade tumors (Gleason score ≥7; n=15), significant differences were observed for the time shift (Δt) between carcinoma and adjacent normal PZ: the signal enhancement started significantly earlier in high- than in low-grade tumors (–9.0±22.9 vs 6.4±7.2 s; p=0.025; Fig. 6). On the other hand, A- as well as k_{21} values from low- and high-grade tumors did not differ.

Discussion

For individual planning, monitoring, and optimization of treatment strategies improved prostate cancer imaging strategies are necessary for tumor characterization. Particularly, there is a great need to distinguish slowly growing from aggressive tumors, which may early progress to present clinically and need to be eradicated by radical prostatectomy. The Gleason grading system evaluating the glandular architecture is the most commonly used grading system for estimating the likelihood of individual tumor aggressiveness; however, tumor aggressiveness cannot be predicted using histopathological criteria alone.

Associations of tumor progression and vascular density have been demonstrated for a variety of human tumors, e.g., breast [21] and cervical cancer [22]. The literature contains several studies regarding the prognostic value of MVD in prostate cancer, which was first noted by Weidner et al. in 1993 [9]. A correlation was reported of intratumoral MVD with tumor progression or recurrence-free survival [11, 12, 23], disease-specific survival [10, 24, 25], and incidence of metastatic disease [9]. But there are also conflicting studies published, which did not find prognostic significance [26, 27].

Conventional contrast-enhanced T1-weighted MRI after intravenous administration of Gd-DTPA does not improve overall staging accuracy as compared with T2-weighted MRI alone [4]. Image interpretation is limited due to strong enhancement of the normal prostate (pronounced in the central zone) as well as an inhomogeneous enhancement in case of BPH, which is very often present in the age group of most prostate cancer patients [28]. On the other hand, dynamic, contrast-enhanced MRI has been shown to be of additional value for tumor detection and staging, particularly in the peripheral zone of the prostate [29, 30, 31, 32, 33].

Fast dynamic, contrast-enhanced MRI with high temporal resolution enables quantification of particularly early contrast enhancement characteristics and assessment of parameters of microcirculation [34]. The underlying mechanisms causing different enhancement curves after intravenous Gd-DTPA administration are complex and depend on tissue specific factors which include the number, perfusion, and permeability of the microvessels as well as the cellular density and the size and physicochemical composition of the extracellular space, in which the contrast media is distributed. In our study, signal–time data from DCE MRI were analyzed using a pharmacokinetic open two-compartment model [18, 19]. According to this model Gd-DTPA enters after intravenous administration the intravascular space (compartment 1), and reaches the tissue by circulation. Dependent on tissue perfusion and microvascular permeability, it passes into the interstitial space (compartment 2) and reenters into the intravascular space, which can be described with a linear exchange processes in both directions [18]. The first-order rate constants for the transfer of Gd-DTPA from the intravascular (interstitial) to the interstitial (intravascular) space is defined as k_{12} (k_{21}). Gd-DTPA is finally eliminated from the intravascular space by the kidneys described by the first-order rate constant k_{el}.

On the basis of our patient population, a correlation was found between the tissue-specific transport parameter k_{21} and the tumor microvessel density quantified by counting (MVC) as well as determining the area fraction

(MVAF). This correlation is reasonable because k_{21} depends on perfusion and vascular permeability [18], which is expected to be increased in tumor areas with higher microvessel density. Furthermore, the observed early signal enhancement of high-grade tumors in the peripheral zone point to an increased permeability and/or total area of perfused vessels within the tumor as compared with low-grade tumors and the adjacent normal prostate tissue (Fig. 6). Accordingly, Padhani et al. reported a delayed onset of signal enhancement after contrast administration in the normal peripheral zone compared with the tumor [32]. Rouvière et al. found that prostate cancer enhanced more and earlier than peripheral zone and adenoma [35]. An increase of mean tumor maximal signal intensity and mean tumor rise time was observed by Preziosi et al. [36]. In a study performed by Tanaka et al., tumor detection was possible in some cases only by identifying areas of early contrast enhancement [31]. Turnbull et al. found significant differences of contrast exchange rate constants also between tumor and BPH [37].

No differences of the amplitude in tumor and uninvolved PZ or CZ and no correlation between the amplitude and MVD in tumor areas were observed (Figs. 4a, 5a). In line with our observations, Padhani et al. found a complete overlap of enhancement patterns of tumor and normal-appearing tissue in the CZ [32]; however, an increased signal enhancement in tumor compared with peripheral zone tissue was reported by Rouvière et al. [35] and Preziosi et al. [36].

The measurement of the contrast exchange-rate parameter k_{21} may be helpful for assessing the prognostic index, because it was found to be correlated with MVD (Fig. 5b). It is important to note that histopathological assessment of the number of small vessels alone may not be a sufficient indicator of angiogenic activity, because it does not necessarily reflect functional microvascular characteristics such as perfusion or vessel wall leakage [26]. Moreover, accurate preoperative assessment of MVD by needle biopsy is problematic due to tumor heterogeneity but may be improved using DCE MRI, which may guide biopsy by identifying areas of high vascular density (hot spots).

Published DCE MRI studies of prostate cancer were performed with different MR sequences including spin-echo and 2D saturation or inversion recovery turbo-FLASH MR sequences. Jager et al. detected early and rapidly accelerating signal enhancement of prostate cancer by using a magnetization-prepared turbo-FLASH sequence with an inversion pulse [29]. In our study, significant differences in enhancement patterns of tumor and normal tissue were detected by using an inversion recovery turbo-FLASH sequence. It is a shortcoming, however, that a linear relationship between the measured MR signal changes and the Gd-DTPA tissue concentration was not experimentally verified for the applied DCE MRI sequence, as this was done for a saturation recovery turbo-FLASH sequence by Hoffmann et al. [20]. Because enhancement characteristics depend on the employed DCE MRI sequence [38], results of different MR examinations can be compared only in cases of comparable examination protocols.

Another shortcoming of our study is that the accuracy of the measured pharmacokinetic parameters may be influenced by the relatively low temporal resolution of DCE MR imaging (13 s/repetition). Additionally, no measurements were performed for the start enhancement time of main arteries in the plane of the tumoral lesion (lag time), which may correct for individual differences in circulation time; however, differences of time shifts between the start of Gd-DTPA administration and signal enhancement do not impair k_{21} values using the method of Brix et al. [18], because time shifts are separately fitted as an independent parameter. It is important to note that the shape of the signal intensity–time curve is determined only by the kinetic parameters k_{21} and k_{el}, whereby the influence of the systemic parameter k_{el} is largely negligible during the initial wash-in phase, from which the parameter k_{21} is eliminated [18]. The "wash-out" is not a separate fit parameter using this model.

The use of MR sequences with higher temporal resolution and new methods of curve fitting may enable a faster and more accurate evaluation of contrast-enhancement characteristics, particularly of the wash-out phase [38], which has been shown to be a predictor of malignancy in breast tumors. The use of macromolecular contrast media may further improve sensitivity and diagnostic accuracy of DCE MRI [39].

Conclusion

Dynamic contrast-enhanced MRI has the potential to provide important information about individual MVD in prostate cancer. The use of DCE MRI to detect differences in perfusion parameters may be helpful for guiding biopsy and assessing individual prognosis.

Acknowledgements We are grateful to M. Späth and A. Kappeler for technical assistance.

References

1. Landis SH, Murray T, Bolden S, Wingo PA (1998) Cancer statistics. CA Cancer J Clin 48:6–29
2. Carter HB, Coffey DS (1990) The prostate: an increasing medical problem. Prostate 16:39–48
3. Sarma AV, Schottenfeld D (2002) Prostate cancer incidence, mortality, and survival trends in the United States: 1981–2001. Semin Urol Oncol 20:3–9

4. Quinn SF, Franzini DA, Demlow TA, Rosencrantz DR, Kim J, Hanna RM, Szumowski J (1994) MR imaging of prostate cancer with an endorectal surface coil technique: correlation with whole-mount specimens. Radiology 190:323–327
5. Yu KK, Hricak H, Alagappan R, Chernoff DM, Bacchetti P, Zaloudek CJ (1997) Detection of extracapsular extension of prostate carcinoma with endorectal and phased-array coil MR imaging: multivariate feature analysis. Radiology 202:697–702
6. Jager GJ, Severens JL, Thornbury JR, Rosette JJ de la, Ruijs SH, Barentsz JO (2000) Prostate cancer staging: should MR imaging be used? A decision analytic approach. Radiology 215:445–451
7. Kurhanewicz J, Vigneron DB, Males RG, Swanson MG, Yu KK, Hricak H (2000) The prostate: MR imaging and spectroscopy. Present and future. Radiol Clin North Am 38:115–138
8. Bostwick DG, Grignon DJ, Hammond ME, Amin MB, Cohen M, Crawford D, Gospadarowicz M, Kaplan RS, Miller DS, Montironi R, Pajak TF, Pollack A, Srigley JR, Yarbro JW (2000) Prognostic factors in prostate cancer. College of American Pathologists Consensus Statement 1999. Arch Pathol Lab Med 124:995–1000
9. Weidner N, Carroll PR, Flax J, Blumenfeld W, Folkman J (1993) Tumor angiogenesis correlates with metastasis in invasive prostate carcinoma. Am J Pathol 143:401–409
10. Mehta R, Kyshtoobayeva A, Kurosaki T, Small EJ, Kim H, Stroup R, McLaren CE, Li KT, Fruehauf JP (2001) Independent association of angiogenesis index with outcome in prostate cancer. Clin Cancer Res 7:81–88
11. Taille A de la, Katz AE, Bagiella E, Buttyan R, Sharir S, Olsson CA, Burchardt T, Ennis RD, Rubin MA (2000) Microvessel density as a predictor of PSA recurrence after radical prostatectomy: a comparison of CD34 and CD31. Am J Clin Pathol 113:555–562
12. Bettencourt MC, Bauer JJ, Sesterhenn IA, Connelly RR, Moul JW (1998) CD34 immunohistochemical assessment of angiogenesis as a prognostic marker for prostate cancer recurrence after radical prostatectomy. J Urol 160:459–465
13. White S, Hricak H, Forstner R, Kurhanewicz J, Vigneron DB, Zaloudek CJ, Weiss JM, Narayan P, Carroll PR (1995) Prostate cancer: effect of postbiopsy hemorrhage on interpretation of MR images. Radiology 195:385–390
14. True LD (1994) Surgical pathology examination of the prostate gland: practice survey by American society of clinical pathologists. Am J Clin Pathol 102:572–579
15. Gleason DF, Mellinger GT (1974) Prediction of prognosis for prostatic adenocarcinoma by combined histological grading and clinical staging. J Urol 111:58–64
16. Grobholz R, Bohrer MH, Siegsmund M, Jünemann K-P, Bleyl U, Woenckhaus M (2000) Correlation between neovascularisation and neuroendocrine differentiation in prostatic carcinoma. Pathol Res Pract 196:277–284
17. Jaeger TM, Weidner N, Chew K, Moore DH, Kerschmann RL, Waldman FM, Carroll PR (1995) Tumor angiogenesis correlates with lymph node metastases in invasive bladder cancer. J Urol 154:69–71
18. Brix G, Semmler W, Port R, Schad LR, Layer G, Lorenz WJ (1991) Pharmacokinetic parameters in CNS Gd-DTPA-enhanced MR imaging. J Comput Assist Tomogr 15:621–628
19. Port RE, Knopp MV, Hoffmann U, Milker-Zabel S, Brix G (1999) Multicompartment analysis of gadolinium chelate kinetics: blood-tissue exchange in mammary tumors as monitored by dynamic MR imaging. J Magn Reson Imaging 10:233–241
20. Hoffmann U, Brix G, Knopp MV, Hess T, Lorenz WJ (1995) Pharmacokinetic mapping of the breast: a new method for dynamic MR mammography. Magn Reson Med 33:506–514
21. Toi M, Kashitani J, Tominaga T (1993) Tumor angiogenesis is an independent prognostic indicator in primary breast carcinoma. Int J Cancer 55:371–374
22. Schlenger K, Hockel M, Mitze M, Schaffer U, Weikel W, Knapstein PG, Lambert A (1995) Tumor vascularity: a novel prognostic factor in advanced cervical carcinoma. Gynecol Oncol 57–66
23. Silberman MA, Partin AW, Veltri RW, Epstein JI (1997) Tumor angiogenesis correlates with progression after radical prostatectomy but not with pathologic stage in Gleason sum 5 to 7 adenocarcinoma of the prostate. Cancer 79:772–779
24. Borre M, Offersen BV, Nerstrom B, Overgaard J (1998) Microvessel density predicts survival in prostate cancer patients subjected to watchful waiting. Br J Cancer 78:940–944
25. Borre M, Nerstrom B, Overgaard J (2000) Association between immunohistochemical expression of vascular endothelial growth factor (VEGF), VEGF-expressing neuroendocrine-differentiated tumor cells, and outcome in prostate cancer patients subjected to watchful waiting. Clin Cancer Res 1882–1890
26. Rubin MA, Buyyounouski M, Bagiella E, Sharir S, Neugut A, Benson M, Taille A de la, Katz AE, Olsson CA, Ennis RD (1999) Microvessel density in prostate cancer: lack of correlation with tumor grade, pathologic stage, and clinical outcome. Urology 53:542–547
27. Gettman MT, Bergstralh EJ, Blute M, Zincke H, Bostwick DG (1998) Prediction of patient outcome in pathologic stage T2 adenocarcinoma of the prostate: lack of significance for microvessel density analysis. Urology 51:79–85
28. Brown G, Macvicar DA, Ayton V, Husband JE (1999) The role of intravenous contrast enhancement in magnetic resonance imaging of prostatic carcinoma. Clin Radiol 50:601–606
29. Jager GJ, Ruijter ET, van de Kaa CA, Rosette JJ de la, Oosterhof GO, Thornbury JR, Ruijs SH, Barentsz JO (1997) Dynamic TurboFLASH subtraction technique for contrast-enhanced MR imaging of the prostate: correlation with histopathologic results. Radiology 203:645–652
30. Barentsz JO, Engelbrecht M, Jager GJ, Witjes JA, Rosette J de la, van der Sanden BP, Huisman HJ, Heerschap A (1999) Fast dynamic gadolinium-enhanced MR imaging of urinary bladder and prostate cancer. J Magn Reson Imaging 10:295–304
31. Tanaka N, Samma S, Joko M, Akiyama T, Takewa M, Kitano S, Okajima E (1999) Diagnostic usefulness of endorectal magnetic resonance imaging with dynamic contrast-enhancement in patients with localized prostate cancer: mapping studies with biopsy specimens. Int J Urol 6:593–599
32. Padhani AR, Gapinski CJ, Macvicar DA, Parker GJ, Suckling J, Revell PB, Leach MO, Dearnaley DP, Husband JE (2000) Dynamic contrast-enhanced MRI of prostate cancer: correlation with morphology and tumour stage, histological grade and PSA. Clin Radiol 55:99–109
33. Ogura K, Maekawa S, Okubo K, Aoki Y, Okada T, Oda K, Watanabe Y, Tsukayama C, Arai Y (2001) Dynamic endorectal magnetic resonance imaging for local staging and detection of neurovascular bundle involvement of prostate cancer: correlation with histopathologic results. Urology 57:721–726
34. Taylor JS, Tofts PS, Port R, Evelhoch JL, Knopp MV, Reddick WE, Runge VM, Mayr N (1999) MR imaging of tumor microcirculation: promise for the new millenium. J Magn Reson Imaging 10:903–907

35. Rouvière O, Raudrant A, Ecochard R, Colin-Pangaud C, Pasquiou C, Bouvier R, Maréchal JM, Lyonnet D (2003) Characterization of time-enhancement curves of benign and malignant prostate tissue at dynamic MR imaging. Eur Radiol 13:931–942
36. Preziosi P, Orlachio A, Giambattista GD, Renzi PD, Bortolotti L, Fabiano A, Cruciani E, Pasqualetti P (2003) Enhancement patterns of prostate cancer in dynamic MRI. Eur Radiol 13:925–930
37. Turnbull LW, Buckley DL, Turnbull LS, Liney GP, Knowles AJ (1999) Differentiation of prostatic carcinoma and benign prostatic hyperplasia: correlation between dynamic Gd-DTPA-enhanced MR imaging and histopathology. J Magn Reson Imaging 9:311–316
38. Huisman HJ, Engelbrecht MR, Barentsz JO (2001) Accurate estimation of pharmacokinetic contrast-enhanced dynamic MRI parameters of the prostate. J Magn Reson Imaging 13:607–614
39. Gossmann A, Okuhata Y, Shames DM, Helbich TH, Roberts TP, Wendland MF, Huber S, Brasch RC (1999) Prostate cancer tumor grade differentiation with dynamic contrast-enhanced MR imaging in the rat: comparison of macromolecular and small-molecular contrast media—preliminary experience. Radiology 213:265–272